



# Lab on a Chip

**Fabrication of 3D concentric amphiphilic microparticles to form uniform nanoliter reaction volumes for amplified affinity assays**

Journal:	<i>Lab on a Chip</i>
Manuscript ID	LC-ART-07-2020-000698.R1
Article Type:	Paper
Date Submitted by the Author:	20-Aug-2020
Complete List of Authors:	Destgeer, Ghulam; UCLA, Department of Bioengineering Ouyang, Mengxing; UCLA, Bioengineering Wu, Chueh-Yu; UCLA, Bioengineering Di Carlo, Dino; UCLA, Bioengineering

SCHOLARONE™  
Manuscripts

# Fabrication of 3D concentric amphiphilic microparticles to form uniform nanoliter reaction volumes for amplified affinity assays

*Ghulam Destgeer,<sup>†, a</sup> Mengxing Ouyang,<sup>†, a</sup> Chueh-Yu Wu,<sup>a</sup> and Dino Di Carlo<sup>\*, a, b</sup>*

<sup>a</sup> Department of Bioengineering, University of California, Los Angeles, CA 90095, USA

<sup>b</sup> Department of Mechanical and Aerospace Engineering, University of California, Los Angeles, CA 90095

<sup>b</sup> California NanoSystems Institute, University of California, Los Angeles, CA 90095

<sup>b</sup> Jonsson Comprehensive Cancer Center, University of California, Los Angeles, CA 90095

KEYWORDS: nanoliter droplets, immunoassay, polymerization, amphiphilic particles, lab on a particle, emulsion, 3D printing, swarm sensing

ABSTRACT: Reactions performed in uniform microscale volumes have enabled numerous applications in the analysis of rare entities (e.g. cells and molecules). Here, highly monodisperse aqueous droplets are formed by simply mixing microscale multi-material particles, consisting of concentric hydrophobic outer and hydrophilic inner layers, with oil and water. The particles are manufactured in batch using a 3D printed device to co-flow four concentric streams of polymer precursors which are polymerized with UV light. The cross-sectional shapes of the particles are altered by microfluidic nozzle design in the 3D printed device. Once a particle encapsulates an aqueous volume, each “dropicle” provides uniform compartmentalization and customizable shape-coding for each sample volume to enable multiplexing of uniform reactions in a scalable manner.

We implement an enzymatically-amplified immunoassay using the dropicle system, yielding a detection limit of  $<1$  pM with a dynamic range of at least 3 orders of magnitude. Multiplexing using two types of shape-coded particles was demonstrated without cross talk, laying a foundation for democratized single-entity assays.

## 1. Introduction

Breaking a sample volume into numerous small compartments enables the accumulation of signal from a small number of molecules or cells to detectable levels in a reasonable time period. Uniformity in the compartment volumes ensures the reaction conditions are relatively similar and reactions across volumes can be compared. Microfluidic wells<sup>[1-3]</sup> or droplet generators<sup>[4-6]</sup> enable uniform compartmentalization of a sample fluid volume into many smaller reactions, however skilled users or specialized and costly commercial instruments have been required for reproducible implementation. In addition, for many affinity assays, a solid phase, such as microbeads, is desired to bind a target and allow washing to remove excess reagents or minimize non-specific binding. A solid phase also allows barcoding for multiplex detection, either by the shape<sup>[7-9]</sup> and/or color<sup>[10-12]</sup> and binding and growth of adherent cells.<sup>[13]</sup> However, introducing a microbead into a well or droplet may introduce other challenges associated with uniform loading of compartments.

Droplet microfluidics is a commonly used compartmentalization technique to disperse aqueous assay reagents with cells or molecules into small segmented volumes inside a continuous oil phase for subsequent signal amplification and detection without cross talk.<sup>[5]</sup> However, encapsulating a single microbead as a solid phase inside each droplet is limited by Poisson loading statistics.<sup>[14]</sup> Therefore, the success rate for encapsulating a combination of exactly two

distinct components i.e. a microbead and a target cell or molecule inside a droplet approaches ~1% of the entire population of droplets, whereas the remaining droplets would have undesired combinations of the components.<sup>[4,15,16]</sup> Moreover, for multiplexing, multiple types of microbeads with distinct barcoding signatures should be encapsulated in separate droplets with the targets of interest, which is further limited by multiplicative probabilities to triple or larger Poisson distributions for duplex or greater multiplexing. Therefore, an instrument-free compartmentalization system that forms uniform droplets embedded with a single solid phase per droplet can address many of the challenges with current approaches.

An attractive alternative technique to create homogeneous compartments uses uniform engineered microparticles to form aqueous volumes by simple exchange of fluids. However, monolithic creation of particles that have structures and material chemistries tuned to spontaneously collect defined uniform aqueous volumes in an oil continuous phase is challenging, and has not yet been reported to our knowledge. Spherical gel beads have been vigorously mixed with aqueous solutions and chemical surfactants to create aqueous volumes occupying a thin shell around the bead, however uniform drops are not at an interfacial energy minimum of the system, while the absence of a cavity has precluded use with mammalian cells and may inhibit some reactions.<sup>[17,18]</sup> In addition, spherical particles have more limited barcoding options, and it has been reported that the presence of surfactants leads to higher rates of transport of products of reactions through the continuous oil phase, reducing sensitivity of enzymatic assays.<sup>[19,20]</sup>

A range of fabrication methodologies have been explored over the past decade to create particles with different shapes and functionalities using continuous<sup>[21–25]</sup> or stop flow lithography techniques<sup>[26–29]</sup> combined with hydrodynamic focusing,<sup>[30–33]</sup> magnetically tunable color

printing,<sup>[12,34]</sup> vertical flows,<sup>[35,36]</sup> structured hollow fibers<sup>[37]</sup> or inertial forces.<sup>[38–41]</sup> However, co-flowing immiscible polymer precursors to create multi-material amphiphilic particles with desired structures is challenging because of the hydrodynamic instabilities that lead to the formation of segmented droplets and subsequently Janus particles.<sup>[42,43]</sup> Particles comprised of layers of hydrophobic and hydrophilic materials were shown to selectively interact and assemble around aqueous drops.<sup>[23,44]</sup> However, these approaches either do not hold a uniform volume of a compartmentalized aqueous phase<sup>[23]</sup> or suffer from a low throughput and complicated fabrication workflow (Table S1).<sup>[44]</sup> In addition, most of these techniques depend on a thin polymerization-inhibition layer close to the walls of oxygen-permeable polydimethylsiloxane (PDMS) microfluidic channels that require cleanroom fabrication facilities. Alternative techniques to shape precursor flows using inertial flow sculpting<sup>[40]</sup> removes limitations on an oxygen-permeable PDMS layer but consumes more reagents per particle fabricated and requires high-pressure flow, whereas vertical flow lithography<sup>[35]</sup> and maskless lithography<sup>[44,45]</sup> that have the capability to create multi-layer 3D particles, suffer from a limited throughput.

Here, we use a 3D printed microfluidic channel network to create particles with an amphiphilic chemistry and a concentric ring-shaped geometry we hypothesized would encompass a uniform volume of aqueous phase inside a hydrophilic cavity of the particle. By using 3D printed concentrically stacked channels, manufactured without cleanroom facilities, we achieve a hydrodynamically focused co-axial flow of hydrophobic poly(propylene glycol) diacrylate (PPGDA) and hydrophilic poly(ethylene glycol) diacrylate (PEGDA) polymers. Otherwise immiscible, PPGDA and PEGDA, when diluted in ethanol, become miscible to flow together without instabilities which is essential to the co-axial flow structure of the streams and concentric shapes of the particles to be fabricated. Co-flowing curable polymer precursor streams with

photo-initiator (PI) are exposed to UV light through a photomask to create concentric particles, whereas an inert outer sheath flow prevents the particles from sticking to the glass capillary walls and an inert inner sheath flow defines the open cavity of the particle. The size of the particle (i.e., 340-400  $\mu\text{m}$ ) and the cavity (i.e., 100-200  $\mu\text{m}$ ) are readily controlled by adjusting the PPGDA to PEGDA flow rate ratio (i.e., 4:1), whereas the shapes of the particles are modulated based on the 3D printed channel designs.

These multi-material concentric amphiphilic particles in which we further functionalize the inner layer to capture target molecules are shown to spontaneously form uniform aqueous drops with assay reagents upon solution exchange. The inner hydrophilic surface of the particle associates with the aqueous phase while the outer hydrophobic surface prefers the oil phase upon exchange to an oil continuous phase. Given the energetic stability of this configuration, simple transfer steps of aqueous reagents with the amphiphilic particles yields uniform aqueous volumes, without the need for control of drop breakup mechanisms that employ precise control of flow rates or pressures. The aqueous drops contain assay reagents surrounded by a continuous oil phase that prevents cross talk during long-duration reactions, while the solid substrate of the templating particle provides an anchor for capturing target molecules. The need for encapsulating an additional particle inside the droplet is also eliminated, thus reducing the effect of Poisson statistics on encapsulation performance.

We conduct an amplified assay using standard reagents for enzyme linked immunosorbent assays (ELISA) within droplets formed by these amphiphilic particles and achieve a sub-pM detection limit with wide dynamic range by accumulating results from hundreds of parallel reactions. A collection of droplets, each acting as part of a “swarm” of individual sensors,<sup>[46]</sup> improves the statistical accuracy in quantitative prediction of concentration by averaging out

small differences in reactions across the droplets. Reactions proceeding simultaneously in two different types of shape-coded particles, separately functionalized, yield minimal cross talk. Tunable assay performance (i.e. detection limit and dynamic range) is also achieved by adjusting the particle dimensions and materials, which is desirable for multiplex detection of biomarkers spanning a large range of clinically relevant concentrations.

## 2. Results

### 2.1. Amphiphilic, Shape-Coded, and Size-Tunable Particle Fabrication

We develop a new approach, leveraging 3D printing, in order to fabricate uniform particles comprising concentric materials of different hydrophobicity. By using a 3D printed microfluidic network of channels, we are able to route four density matched precursor fluids with different chemistries, an inert outer sheath (PPGDA only, or PPG and PI), PPGDA and PI, PEGDA and PI, and an inert inner sheath (PEGDA only, or PEG and PI), through four concentric channels to obtain a co-axial flow structure (**Figure 1A, Figure S1**). The internal structure of the microfluidic channels with a tapered geometry at the exit ensures that the flow stream from channel 4 first co-flows with the flow stream from channel 3, which is subsequently combined with the flow streams from channel 2 and 1. To reduce the effect of diffusion of species between streams, the diameter of the device is gradually reduced to increase the flow velocity as the flow streams are merged together in a sequential manner, resulting in a final Peclet number ( $Pe$ ) of  $\sim 5 \times 10^5$ . The fully developed co-axial flow is briefly stopped to expose the polymer precursors to UV light through a patterned array of windows in a photomask to cure multi-material concentric particles (Figure 1C). The cured particles with a hydrophobic outer PPG layer and hydrophilic inner PEG layer are washed downstream to a collection tube as the flow inside the channels is

restarted (Figure 1D). This cycle is repeated automatically to continuously fabricate and collect particles for a desired number of cycles (Figure 1B). The partitioning of fluorescent resorufin into the PEG layer confirms the multi-material composition of the particles (Figure 1E). The reproducible structured co-flow along with automated processing and exposure ensures that each fabrication batch of the particles has a high uniformity in their shape, size and material composition (Figure 1F-G).

Instead of relying on changes to the masked light intersecting the polymer precursor stream we engineer the 3D printed channel structures to tune the cross-sectional flow shapes and produce a variety of shape-coded particles (**Figure 2**). Microfluidic devices that have nozzles designed with different cross-sections (*a-a'*), as indicated in Figure S2A, yield particles with engineered shapes. Particles with shape codes defined in the outer, inner, or both materials are fabricated to demonstrate the capabilities of the 3D printed channels (Figure 2, Figure S2B, Figure S3). For outer shape codes, the four corners of square particles are systematically removed to obtain six different shapes while the inner cavity shape is kept the same (Figure 2C). For inner shape codes, the outer square boundary of particles is maintained, while different distributions of the PEG layer are shaped to form unique internal features (Figure 2D). The outer and inner boundaries of particles are also modified in combination to obtain complex internal and external particle features (Figure 2F). The cross-sectional geometries of shaped particles possess high uniformity with a CV of less than 2% in inner diameter and less than 4% in outer diameter (Figure S2C and Figure S4). Analysis of the inner and outer perimeters and circularities can be used to distinguish different shape-coded particles without errors in the sample size we evaluated (Figure S4). The flow rates for the polymer precursors are also readily adjusted to tune the size of the particles

(Figure S2D, Figure S5). For O-shaped particles, increasing the flow rate ratio ( $Q_{1,2}:Q_{3,4}$ ) from 1 to 4 gradually reduced the size of the particle cavities from  $\sim 185\ \mu\text{m}$  to  $\sim 100\ \mu\text{m}$  (Figure S2D).

## 2.2. Dropicle Formation

Dropicles, uniformly-sized droplets supported by particles, are formed by simple pipetting for fluid phase exchange (Figure 2A). The surrounding fluid phase for the particles is exchanged first from ethanol to phosphate buffered saline (PBS), and then from PBS to a mixture of PBS with aqueous solution (e.g., a fluorophore or color dye solution) for subsequent intensity measurements or droplet visualization. Adding a final oil phase with low interfacial tension with the outer PPG layer creates hundreds of isolated compartments, or dropicles, immediately. As the excess fluid is removed at each step, nanoliter-scale volumes of aqueous solution remain in an energetically favorable configuration associated with the hydrophilic core of the amphiphilic particles. We would like to point out that the leakage of constituents out of droplets has been a general issue for conventional droplet systems, as these systems require the use of surfactant in the oil phase for droplet formation and stabilization.<sup>[19,20]</sup> The surfactants can enhance transport between droplets through micellar transport of hydrophilic compounds which may have low partition coefficients into the oil phase. However, it is worth noting that our system does not need surfactant to form droplets. Instead, the droplet formation is due to the hydrophobicity difference within different layers of the multi-material particles. Droplets formed within the various shape coded particles span the entire inner hydrophilic layer and reflect the shape of the cavities (Figure 2B, Figure S2E). Besides manipulating the outer hydrophobic layer of the amphiphilic particles (Figure 2C), variations in the hydrophilic inner cavity are also engineered (Figure 2D, F), however, these inner and outer shape changes do not appear to affect the ability to hold an aqueous droplet (Figure 2E, G). Particles with different designs can hold 2-6 nL

droplets depending on the shape and size of the cavities, whereas the variation in volume is less than 10% on average and variation in diameter of an equivalent volume spherical droplet is  $\sim 3\%$  (Supporting Information).

### 2.3. Amplified Affinity Assay in Dropicles

The materials and emulsification process used to form dropicles is compatible with affinity assays using enzymatic amplification of signal. We demonstrate a QuantaRed assay within dropicles, in which a fluorogenic precursor (10-Acetyl-3,7-dihydroxyphenoxazine, ADHP) is converted into fluorescent resorufin due to the activity of horse radish peroxidase (HRP) that bound to the surface of biotinylated particles (**Figure 3A**). The assay generally follows standard steps required for conducting ELISAs. Biotinylated particles suspended in ethanol are first added to a well plate with a hydrophobic surface, where they quickly settle on the bottom of the well with the majority facing upward, due to the density difference and aspect ratio of the particles. With a reasonable seeding density, these particles are also well separated without adhering to adjacent particles because of the low interfacial tension between the particles and the continuous phase. Next, the ethanol solution is exchanged with a PBS buffer with an average particle retention rate of 98% through solution exchange and subsequent incubation steps (see Supporting Information for details). Then, streptavidin-HRP solution was added and incubated for 30 min, leading to HRP binding to particles. Following HRP binding and thorough washing similar to that of standard ELISA (see Experimental Section for details), QuantaRed solution is loaded into the well with excess removed immediately from the corner of the well. Lastly, oil is added to form and seal the droplets within seconds (see Experimental Section for details). Once in dropicles, ADHP in the QuantaRed solution is catalytically converted by HRP into resorufin which accumulates in the aqueous phase and also partitions to some extent into the encapsulating

PEG layer,<sup>[47,48]</sup> but is not observed to transfer into the oil phase. Fluorescent and bright field images of the droplets while in oil are obtained for a few hundreds of compartmentalized reactions (Figure 3B). Typically, the fluorescent signal from the droplets increases over time (Figure S6) and as expected increases at a higher rate for higher concentrations of streptavidin-HRP (e.g., 10 pM) while remaining constant for a negative control group of particles that are incubated with PBS only. In further validating this assay, we picked specific time points to image and quantify droplet fluorescence after which sufficient fluorescent signal is developed (typically > 15 min).

We observe selective amplification within droplets and minimal cross talk of signals between particles functionalized with an affinity moiety (biotin) and those without. Plus-shaped particles without biotin in the PEGDA layer are used as a negative control population while H-shaped particles with biotin in the PEGDA layer are used as a positive population with high affinity to streptavidin-HRP (**Figure 4A**). Upon incubation together with a relatively high concentration of streptavidin-HRP (0.1 nM) the two populations are easily distinguished in both bright field, based on the structure of polymerized polymer, and fluorescence images (Figure 4B-C). The fluorescent signal from plus-shaped particles (negative group) increases at a much slower rate compared to that of H-shaped particles (positive group) (Figure 4D). The average intensity at 15, 35, and 60 min time points is 9.0, 12.1, and 12.3 fold higher for biotin-modified particles compared to non-modified particles, respectively (Figure 4E). The fluorescence intensity differences for these two mixed particle types over time is consistent with observations for the same particle types that were not mixed together, indicating minimal transport of the produced resorufin dye through the oil phase. Even at 48hrs, although some of the droplets are partially evaporated, the signals from these two particle types remain noticeably different (Figure S7).

These results demonstrating limited cross talk support the potential for multiplexed detection using shape-coded particles.

Using an amplified assay in droplets we achieve a sub-picomolar level detection limit while maintaining a wide dynamic range. In addition, the solid substrate templating the droplet provides flexibility in adjusting the number of binding sites per particle. We report results from a concentration sweep of streptavidin-HRP for two biotinylated particle types. Particle Design 1 has an extruded height of 200  $\mu\text{m}$  and a  $\sim 2$ -fold thicker PEGDA layer compared to particle Design 2 which has a height of 100  $\mu\text{m}$  and thinner PEGDA layer (**Figure 5A**). Both particle designs achieved  $< 1$  pM detection limit with an at least 4-orders-of-magnitude dynamic range (Figure 5B-C). In comparison, Design 1 exhibits a detection limit of 100 fM, and linear range from 1 pM to 1 nM (3 orders of magnitude,  $R^2 = 0.9983$ ). Design 2 exhibits an improved detection limit of 10 fM, but a narrower linear range from 1 pM to 100 pM (2 orders of magnitude,  $R^2 = 0.9815$ ). The detection limit was experimentally determined as the lowest statistically differentiable concentration (with  $> 99.9\%$  confidence level, i.e.,  $p < 0.001$  using student's t-test) between the population of particles with droplets containing an analyte concentration versus droplets exposed to the same workflow but without analyte. Notably, amplified assays in droplets from both designs outperformed direct binding of fluorescent streptavidin to the particles (Figure S8). Direct binding of streptavidin-Alexa Fluor<sup>®</sup> 568, using the same particles as shown in Figure 5C, led to a weaker signal, requiring at least 1nM of streptavidin for detection, equivalent to a 5-orders-of-magnitude signal enhancement with the same number of binding sites per particle. This suggests that signal amplification is important to maximize the capabilities of particle-based assays.

Furthermore, the amplified dropicle assay flow was adapted to a sandwich ELISA workflow for the detection of N-terminal propeptide B-type natriuretic peptide (NT-proBNP), a guideline recommended biomarker for cardiovascular disease (Figure 5D). The dropicle system achieved a detection limit of 10 pg/ml (i.e., 285 fM) and the highest sensitivity between 100 pg/ml and 1 ng/ml which corresponds well to the clinically relevant range around a few hundred pg/ml.

### **3. Discussion**

#### **3.1. Instrument-Free Formation of Uniform Compartments**

The dropicle system presented here provides a platform to create uniform nanoliter-scale compartments with existing laboratory equipment and processes. Analyte-specific batches of different shape-coded particles can be manufactured in bulk and easily distributed to life science researchers interested in performing compartmentalized bioassays. We estimate that the material cost to produce 15,000 particles, more than enough for an assay, to be ~\$1 (Supporting Information). There is no need for microfluidics experience or specialized equipment because droplet formation requires only simple pipetting steps typical of a standard ELISA assay workflow. Two additional steps specific to a dropicle workflow are: 1) An initial transfer and media exchange step such that amphiphilic particles stored in ethanol are resuspended in an aqueous solution. 2) A final step following addition of a readout solution, such as QuantaRed, in which excess solution is removed immediately from the well plate and oil is added on top of the particles to seal the droplets formed. Both of these steps are simply achieved using typical pipetting techniques within 1-2 min, therefore no additional training or instruments are needed for novice users to implement sophisticated nanoliter-scale compartmentalized reactions. For more experienced researchers interested in fabricating the reported particles or customizing

them, the 3D printed device designs we use, which we have made freely available (Supporting Information), can be outsourced to a number of vendors and received within a few days. For customized particle designs, users can tune the co-axial channel cross-sections and the photomask to change the shape and thickness of the particles, respectively.

### **3.2. Improved Detection Accuracy Through Swarm Sensing**

Hundreds of dropicles can be read in a single well, enabling swarm sensing.<sup>[46]</sup> Biosensing accuracy suffers from low signal above background at low analyte levels and random variations in sensor performance at higher analyte levels which limit quantitation. Conventional detection schemes, such as ELISA, overcome low analyte level challenges through enzymatic signal amplification, however these assays typically measure the bulk signal from a single or few reactions, leading to compromised detection sensitivity and accuracy. When reading out reactions in dropicles, signal intensity is affected by a number of random factors including variations in particle manufacturing, variations in droplet volume, non-specific binding, and measurement noise introduced by the excitation and readout system. Accumulated random errors are significantly reduced by compiling a histogram or summary statistics of the independent signals from a large number of particles in the well (i.e., larger swarm size, Figure S9A). Accumulating these data results in a statistically robust determination of the ground truth signal, which can lead to a more robust and accurate quantification of concentration. For example, when sample size was increased from  $n=3$  dropicles to  $n=300$ , the standard error, which is a measure of the accuracy of the sample mean compared to the population mean, was significantly improved (i.e., decreased  $\sim 7$ - $16$  fold for various concentrations with an average of  $\sim 12$  fold, Figure S9B). Using information about expectations for the distribution of results for a given ground truth can also yield enhanced prediction capabilities<sup>[49]</sup>. Depending on the application,

the sample size (i.e., number of particles per well) could be further scaled up if higher sensing accuracy and detection fidelity are required.

### **3.3. Multiplexing Immunoassays in Dropicles**

Multiplexed detection using microfluidic-based approaches, such as microbeads encapsulated in droplets, are limited in scale by multi-Poisson statistics. The loading efficiency of droplets with a desired combination of barcoded solid phase particles (i.e. only a single type per droplet) is expected to decrease drastically as the number of targets in the multiplexed panel increases. This inevitably escalates the imaging acquisition burden and prolongs readout time with the need to isolate potential combinations of barcodes for data analysis.<sup>[50]</sup> A potential solution is to further enhance the throughput of the droplet generator and reader<sup>[4]</sup> to shorten the time needed to accumulate a sufficient number of droplets containing only one particle of each single type. Our dropicle system provides an alternative approach to overcome this obstacle, as the single solid phase is designed into the amphiphilic particles during manufacturing, and therefore not subject to Poisson loading statistics.

Moreover, the customizability of particle design using co-axial flow allows for the batch fabrication of a vast collection of individually barcoded particles that can support independent reactions. Once in possession of these encoded “building blocks”, users would benefit from ease of assay modification by mixing and matching different types and numbers of particles as desired, without the use of additional instrumentation. Note, it is challenging to achieve the same level of user flexibility using planar microwell systems with a pre-determined layout, where droplets are either dispensed directly on top of a planar surface,<sup>[51,52]</sup> or encapsulated in small chambers.<sup>[1,2]</sup> In addition, compared to other droplet based systems that often rely on

fluorescent/color based labeling to achieve multiplex detection, our shape-coded particles only require signal readout in a single fluorescence channel together with bright field imaging for multiplex detection, alleviating the need for more complex multi-channel fluorescence readers and the challenges with compensation between fluorescence channels. Therefore, the shape-coded dropicle system is particularly beneficial for cost-effective assays that are compatible with similarly cost-effective readers based on consumer electronic devices,<sup>[53,54]</sup> which paves the way for multiplexed detection at point-of-care settings or other limited resource settings. An analysis of the potential number of distinguishable shapes is discussed in the Supporting Information.

Furthermore, modifying the dimensions (e.g.  $t$  and  $w$  denoted in Figure 5B) and potentially chemistry of the PEGDA layer<sup>[22,30,40]</sup> allows for tuning of the detection limit and dynamic range of an assay for the optimal detection of target analytes in each dropicle. For disease diagnosis, multiplexed *in vitro* assays are often limited by the capability to detect analytes spanning a wide range of clinical cutoffs. For instance, among cardiac biomarkers, the clinical cutoffs range from pg/ml (e.g., cardiac troponins), sub-ng/ml (e.g., natriuretic peptides), ng/ml (e.g., creatine kinase-MB), to  $\mu\text{g/ml}$  (high-sensitivity c-reactive protein).<sup>[55]</sup> To tackle this issue, commercial assays and research platforms focus on the development of either a single assay with a wide dynamic range<sup>[56]</sup> with trade-offs in quantitative accuracy, or a multi-modal sensing approaches to cover different concentration ranges.<sup>[57,58]</sup> Tuning the assay characteristics within each type of barcoded dropicle promises a simpler and more practical approach to achieve the simultaneous detection of multiple markers. In addition, a collection of different shape-coded particles tuned for quantitative accuracy in a particular concentration range could also be utilized to expand the dynamic range for detection of a single marker, minimizing the need for sample enrichment or dilution in a clinical workflow.

### 3.4. Lab on a Particle Systems

By enabling the simple formation of uniform and stable nanoliter compartments in a biocompatible oil phase without cross talk, dropicles can serve as a platform for a variety of molecular and cellular assays leveraging standard laboratory equipment. The enzymatic affinity assay we demonstrate is a foundational component of many ELISA workflows, indicating dropicles should be well-suited for biomarker detection using immobilized antibodies, aptamers, or other affinity elements for *in vitro* diagnostics ultimately approaching single molecules.<sup>[59]</sup> Our system maintains the advantages of amplification that is achievable with bulk assays, while also providing unique benefits of barcoded particle-based assays and smaller volume analysis. Furthermore, it enables rare or low volume sample multiplexed analysis all in one well using enzymatically amplified assays, which is not possible to achieve without the compartmentalization capability. Importantly, analysis of hundreds to thousands of reactions in a single well could lead to the ability to perform more tests with limited sample volume, reduce reagent consumption, and overall assay time, compared to conducting assays in large volume wells. These benefits are particularly attractive for clinical trials, drug screening, and diagnostics, where sample volumes can be small or precious.

Digital nucleic acid detection using compartmentalized amplification of single nucleic acids with PCR or Loop-mediated isothermal amplification (LAMP)<sup>[60]</sup> should also be compatible with dropicle systems given the similar volumes to current systems and biocompatibility of the PEG layer and surrounding oil. In addition, by modifying the PEGDA layer with cell adhesive-moieties such as biotinylated collagen,<sup>[40]</sup> our amphiphilic particles could serve as cell carriers, enabling single cell culture and analysis, including the accumulation of secretions<sup>[61]</sup> or RNA in the small volume of a dropicle for secretion or gene expression analysis.<sup>[62]</sup> For applications

requiring screening of larger numbers of particles, high throughput imaging cytometry could be used.<sup>[63]</sup> Building off this work, we envision such dropicle systems can serve as minimally-instrumented and accessible “lab on a particle” platforms for analysis of molecules and cells at the ultimate limits of biology.

## 4. Experimental Section

### 4.1. Particle Fabrication

The particle manufacturing system comprises a fluidic system with a 3D printed microfluidic device connected to syringe pumps to drive the pre-polymer co-flow, a pinch valve to stop flow, and an optical system in which the co-flow is exposed to patterned UV light through a mask (Figure S1, see Supporting Information for details). Four different streams of density matched solutions are pumped through the 3D printed device inlets 1-4 at flow rates  $Q_1$  to  $Q_4$ , respectively with the syringe pumps, yielding an inlet pressure of  $P_{in}$  (Figure 1A). The net flow rate results in an average velocity of  $U_{avg}$  within the square section of the glass capillary. The pinch valve at the outlet is used to stop the flow entirely ( $U_{avg} = 0$ ) such that the outlet pressure of  $P_{out} (= P_{in})$ , whereas the syringe pumps are simultaneously turned off to cut the flow through the inlets. The shutter is opened after a short delay time ( $\tau_d$ ) to ensure that the flow has fully stopped, whereas the UV light source with intensity  $I_{UV}$  exposes the flow streams through a photomask for an even smaller exposure time ( $\tau_{exp}$ ) (Figure 1C). Co-axial flow streams are exposed to rectangular-shaped UV patterns defined by an array of 20 or 30 slit features (width 100 or 200  $\mu\text{m}$   $\times$  length 1000  $\mu\text{m}$ ) in the photo mask. The width of the UV beam defines the thickness of the polymerized region and the particle, whereas the 1000  $\mu\text{m}$  breadth of the UV beam is enough to cover the whole cross-section of the rectangular glass capillary. The extended breadth of the pattern (1000

$\mu\text{m}$ ) also allows for easy alignment with the glass capillary ( $700\ \mu\text{m}$  outer dimension). The flow streams originating from channels 2 and 3 are polymerized in the form of a ring-shaped amphiphilic particle with hydrophobic outer layer made of PPGDA and hydrophilic inner layer made of PEGDA (Figure 1D). At this point, the pinch valve is opened ( $P_{out} = 0$ ) and the syringe pumps are started again to reach an average flow velocity of  $U_{avg}$  within a flow stabilization time ( $\tau_s$ ). The whole cyclic process of flow stoppage, UV exposure and flow stabilization is further described by plotting  $P_{in}$ ,  $P_{out}$ ,  $I_{UV}$  and  $U_{avg}$  against time and indicating  $\tau_d$ ,  $\tau_{exp}$ , and  $\tau_s$  in Figure 1B. One fabrication cycle is completed within  $\sim 5\text{s}$  for most experimental conditions. An automated experimental setup integrated through a LabVIEW GUI allows for rapid and on-demand control of the parameters ( $\tau_d$ ,  $\tau_{exp}$ ,  $\tau_s$  and  $U_{avg}$ ). The average flow velocity is controlled by adjusting the flow rates for the four inlets  $Q_{1-4}$ .

## 4.2. Dropicle Formation

Dropicles are formed using a simple workflow based on pipetting and washing (Figure 2A). Particles initially suspended (and stored) in ethanol (step 1) are transferred to a hydrophobic well plate where the medium is exchanged to PBS after three washes (step 2). Introduction of an aqueous solution results in swelling of the inner PEG layer thus reducing the inner cavity size to some extent. To characterize the uniformity of droplet volume in dropicles,  $20\ \mu\text{g/ml}$  biotin-4-fluorescein (AnaSpec, CA, USA) dissolved in PBS is added (step 3). Once the aqueous fluorophore solution is fully dispersed around and inside the particle cavity by wetting the hydrophilic inner surface, excess liquid is removed (step 4) while an aqueous phase remains trapped within particle cavities. Poly(dimethylsiloxane-co-diphenylsiloxane) (PSDS, Sigma-Aldrich, MO, USA) oil is added on top of the particles to complete the compartmentalization of the aqueous phase within the hydrated particles by pushing any remnant aqueous phase outside

of the particles away from them (step 5). After the oil is added, the particles gradually recover back to their original shape as the PSDS swells the outer PPG layer in a similar manner as the original ethanol storage solution.

#### **4.3. Amplified Affinity Assay with QuantaRed**

Particles suspended in ethanol are first added to a 12 well plate. Once particles settle in the well excess ethanol is removed, followed by three washes with PBS with 0.5% w/v Pluronic (PBSP). For each washing step, 500 $\mu$ L of washing buffer is added to the center of the well, and subsequently removed from the corner of the well. This process is repeated three times to complete each wash cycle. Then, 300  $\mu$ l of streptavidin-HRP solution at varying concentrations (Thermo Fisher Scientific, MA, USA) is added and incubated for a given time period, followed by three additional washes with PBSP. Next, 500  $\mu$ l QuantaRed solution (Thermo Fisher Scientific, MA, USA) is mixed following the instructions of the vendor (at a 50:50:1 ratio of enhancer solution, stable peroxide, and ADHP concentrate, respectively) and added to the well to wet the particles with excess removed immediately. Lastly, 500  $\mu$ l oil (PSDS) was added to form isolated droplets. Next, fluorescence and bright field images of the droplets in oil are obtained at desired time points using a fluorescence microscope. The excitation and emission maxima of the fluorescent product are at  $\sim$ 570 and 585 nm, respectively. Imaging of the whole well allows the simultaneous monitoring of a few hundreds of reactions in compartmentalized droplets. The same assay protocol was used for assay performance characterization using two types of O-shaped particles. In the negative control group, particles were incubated with PBS only, all the other steps were kept the same as positive groups as described in Figure 3. To determine the fluorescence intensity of the amplified assay, region-of-interests (ROI) are defined within each droplet held within the droplet (excluding the inner PEG layer), and the average intensity was

extracted using ImageJ to represent the amplified signal of each droplet. The very small fraction of particles that are settled on their sides have distinctive shape differences, which allows them to be differentiated from particles facing upwards and excluded from analysis using parameters such as circularity and area.

#### **4.4. Duplex Experiment**

Plus-shaped particles without biotin in the PEG layer are used as a negative control population; H-shaped particles with biotin in the PEG layer are used as a positive population. These two types of particles have different shapes of the outer PPG layer and inner PEG layer, and can therefore be easily distinguished by shape in both bright field and fluorescence channels. Both types of particles are mixed at a 1:1 ratio in ethanol in an Eppendorf tube and subsequently transferred to a well in a 12 well plate. Particles are then washed with PBSP three times, and incubated with 0.1 nM streptavidin-HRP solution for 30 min. Then, the same QuantaRed assay protocol is performed as described above, where particles are washed again, and droplets are subsequently formed encapsulating the QuantaRed mixture.

#### **4.5. NT-proBNP Detection Using Amphiphilic Particles**

We developed a sandwich ELISA for NT-proBNP detection using commercial monoclonal antibodies. A monoclonal capture antibody (15C4cc, HyTest, Finland) was conjugated with biotin, and a monoclonal detector antibody (13G12cc, HyTest, Finland) was conjugated with HRP, respectively, using commercial conjugation kits (Lightning-Link, Expedeon, United Kingdom) following vendor instructions. Particles with biotin were transferred to a well plate in ethanol and washed as described above. To immobilize capture probes onto the particles, 10  $\mu\text{g/ml}$  streptavidin (Thermo Fisher Scientific), MA, USA was added to the well and incubated

for 30 min, followed by three washes. Then, particles were incubated with 10  $\mu\text{g/ml}$  biotin conjugated capture antibody for 1 hr to complete the immobilization step, where unbound antibodies were removed through washing steps. Next, blocking buffer (Thermo Fisher Scientific, MA, USA) was added to the well containing particles and incubated for 1 hr followed by washing. To test the detection of NT-proBNP, particles were incubated with varying concentrations of human recombinant NT-proBNP (HyTest, Finland) for 1 hr with subsequent washing, followed by incubation with 0.5  $\mu\text{g/ml}$  HRP conjugated detector antibody for 1 hr, and a final washing step. Lastly, the QuantaRed assay solution was added for amplification, and droplets were formed in PSDS oil as described above. In the negative control group, particles were incubated with PBS only instead of NT-proBNP, but all the other assay steps, including immobilization, blocking and detection etc., were kept the same as the positive groups. Fluorescent intensity was measured 45 minutes after adding QuantaRed solution.

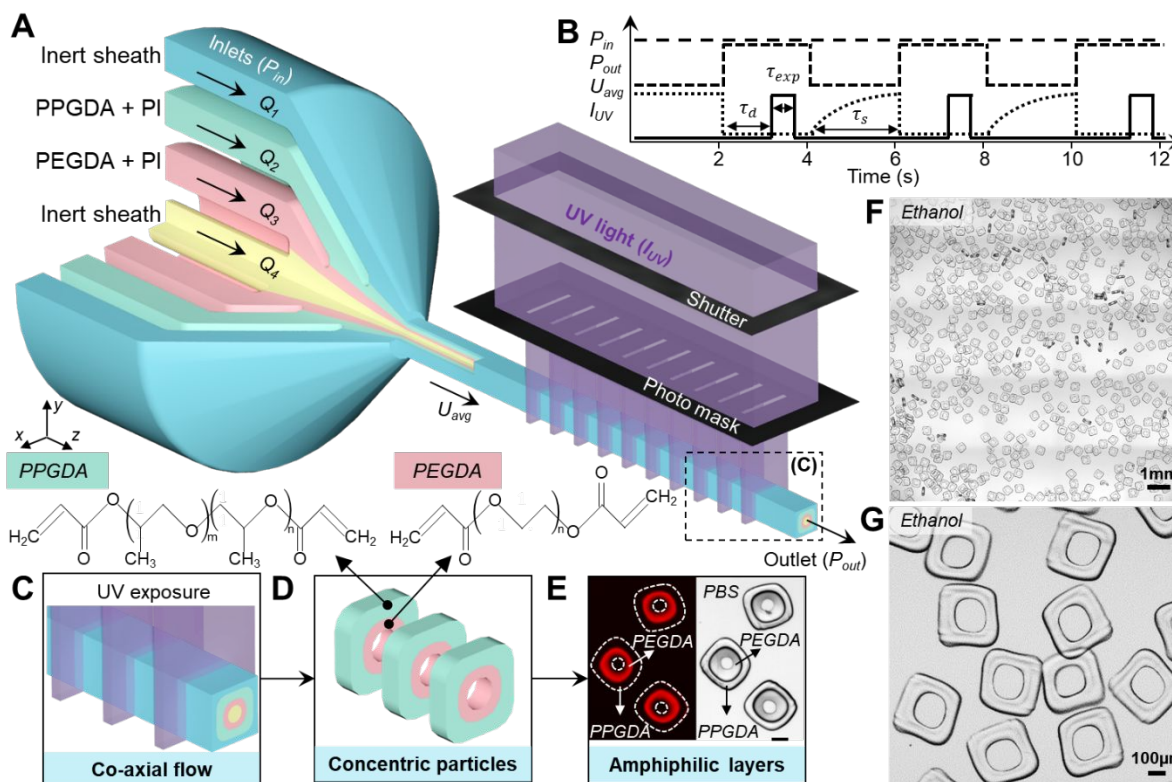


**Figure 1. Fabrication of concentric amphiphilic microparticles.** (A) Four different streams of fluids are pumped through inlets 1-4 at flow rates  $Q_1$  to  $Q_4$ , respectively, resulting in an inlet pressure,  $P_{in}$ . Flow streams from inlets 2 and 3 contain curable polymer pre-cursors mixed with photoinitiator (PI). The flow reaches an average velocity of  $U_{avg}$  within the square section of the device. The flow is stopped ( $U_{avg} = 0$ ) with a pinch valve resulting in an outlet pressure of  $P_{out}$  ( $= P_{in}$ ). A shutter is opened after a short delay time ( $\tau_d$ ) to expose the flow streams to UV light with intensity  $I_{UV}$  through a photomask for an even smaller exposure time ( $\tau_{exp}$ ). At this point, the pinch valve is opened ( $P_{out} = 0$ ) and the syringe pumps are re-started to reach an average flow velocity of  $U_{avg}$  within a flow stabilization time ( $\tau_s$ ). (B) The plot summarizes the whole process of flow stoppage, UV exposure and flow stabilization in a cyclic manner. (C) A zoomed-in view of the exposure region shows that the co-axial streams are exposed to rectangular-shaped UV beams. (D) The curable flow streams are polymerized in the form of a ring-shaped amphiphilic particle with hydrophobic outer layer made of PPGDA and hydrophilic inner layer made of PEGDA. (E) TRITC (left) and bright-field (right) images of representative fabricated particles mixed with resorufin that partitions into the PEG layer are shown. The dashed lines mark the outer boundaries of the particle in the fluorescent image. Scale bar is 100  $\mu$ m. (F) A batch of fabricated O-shaped particles suspended in ethanol shows a high uniformity in the particle size as well as the inner cavity. Scale bar is 1 mm. (G) A zoomed image of the particles suspended in ethanol shows a circular cavity within an outer square-shaped boundary of the particle. Scale bar is 100  $\mu$ m.

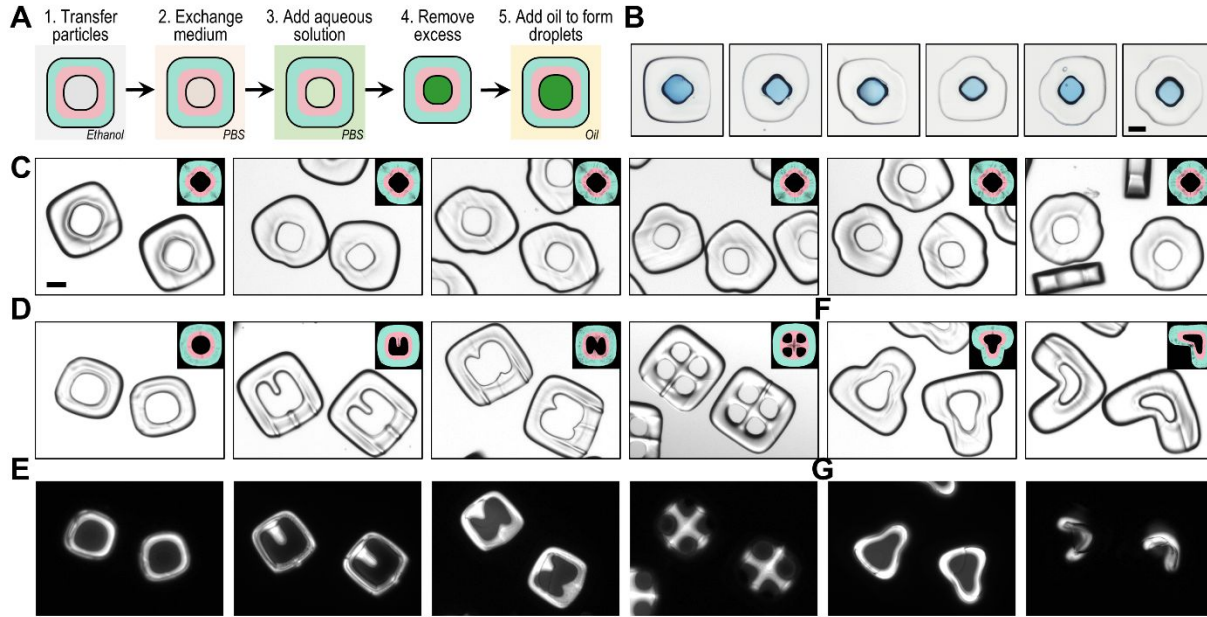


**Figure 2. Shape-coded particles and aqueous droplet formation inside the cavities. (A)** Workflow for droplet formation as amphiphilic particles are transferred from ethanol to PBS before exchanging with an oil continuous phase. **(B)** Droplet formation using six different outer shape coded particles. **(C)** Outer shape code demonstrated by systematically removing combinations of corners from an outer square shaped particle. **(D)** Inner shape coded particles with an outer square shaped boundary. **(E)** Droplet formation inside inner shape coded particles as observed with fluorescence imaging of encapsulated resorufin dye. Partitioning into the inner PEG layer is observed **(F)** Bilayer-shape coded particles with changes reflected in the inner and outer boundaries of the particles. **(G)** Droplet formation inside bilayer-shape coded particles as observed with fluorescence imaging of encapsulated resorufin dye. Scale bars are 100  $\mu\text{m}$ . Insets for (C, D, F) show fluid dynamic simulation results of the cross-sectional shape of the outer PPG layer (cyan) and inner PEG layer (magenta).

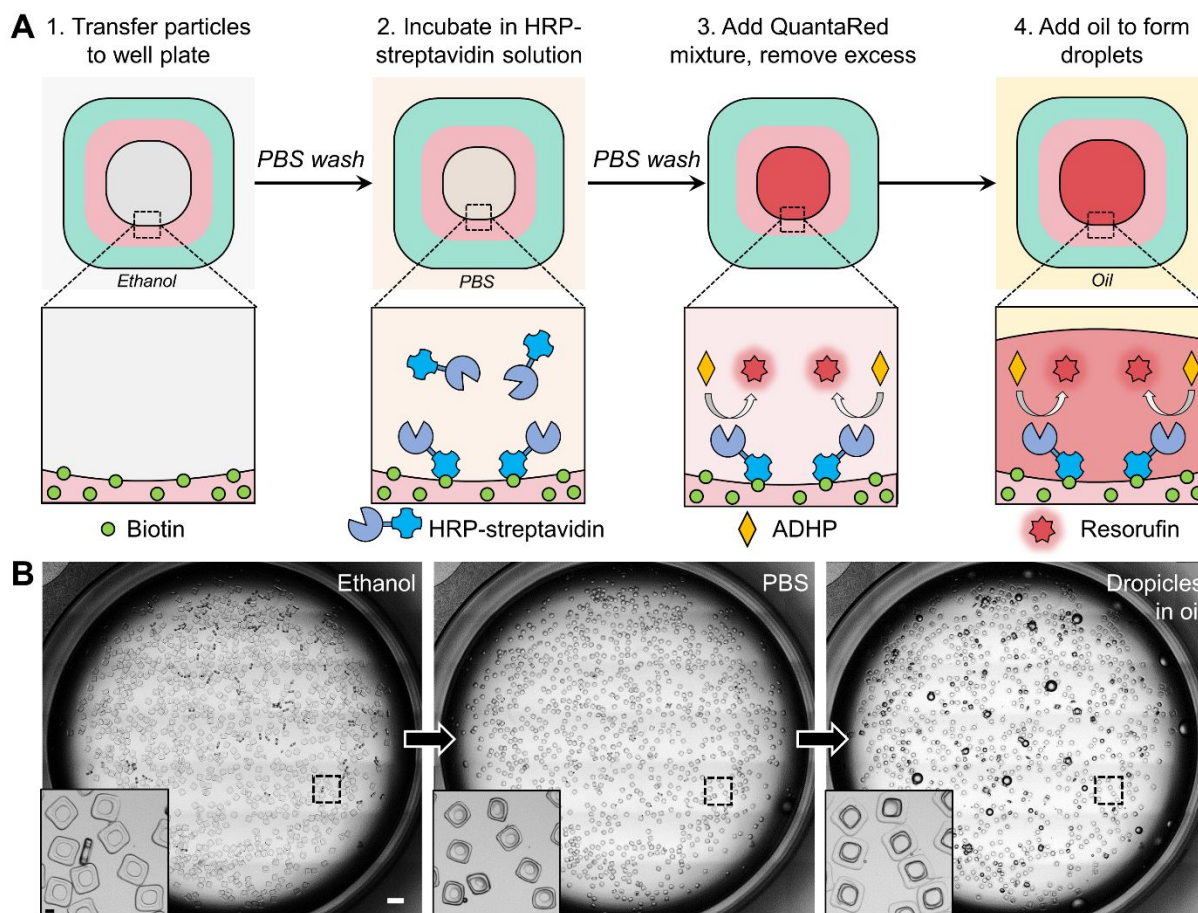


**Figure 3. Amplified bioassay in droplets.** (A) Schematic of the assay workflow for biotin streptavidin affinity and the mechanism of amplification using horse radish peroxidase (HRP) turnover of the fluorogenic substrate ADHP to generate resorufin. (B) Microscopic images of a single well at different steps of the assay workflow. Images are captured when particles are in ethanol (step 1), PBS (step 2), and PSDS oil (step 4) where droplets are formed. Zoomed in inset images of the same field-of-view highlight the particle morphology changes as the inner PEG and outer PPG layers swell or shrink in different solutions. Scale bar for the whole well is 1 mm, and the scale bar for the insets is 100  $\mu\text{m}$ .

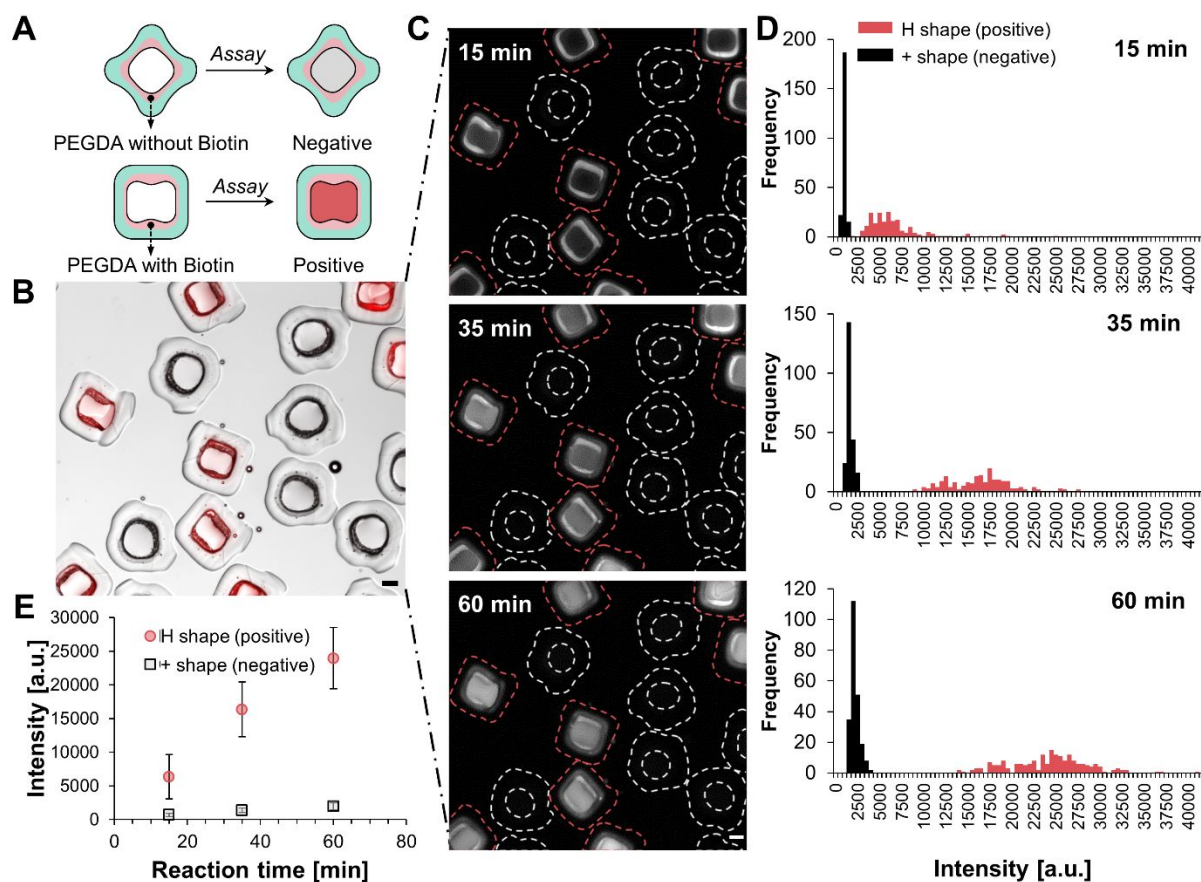


**Figure 4. Duplex assay using shape-coded particles demonstrating minimal cross talk.** (A) Schematic of the duplex assay showing the two particle populations: plus-shaped particles without biotin in the PEGDA layer are used as negative control population; H-shaped particles with biotin in the PEGDA layer are used as a positive population. (B) A merged image of bright field and fluorescent channels, after mixing plus- and H-shaped particles, incubating with 0.1 nM streptavidin-HRP solution, and initiating the HRP amplification reaction. There is contrast in the red fluorescent signal between plus-shaped particles and H-shaped particles. (C) Fluorescence images of the same field of view as in (B) at 15, 35 and 60 min after initiating the reaction. Red dotted lines in the images outline the PPG boundary of H-particles (positive) while white dotted lines outline the PPG boundary of plus-particle (negative). Scale bars in (B-C) represent 100 $\mu$ m. (D) Histograms showing the intensity distribution for a population of plus-shaped and H-shaped droplets at 15, 35 and 60 min. (E) The mean of fluorescent intensity at these three timepoints 15, 35, and 60 min for H- and plus-shaped particles, showing the negative volume does not appear to have an appreciable increase in intensity over time even as the positive volume shows high levels of fluorescence intensity increase. The error bars represent standard deviation.

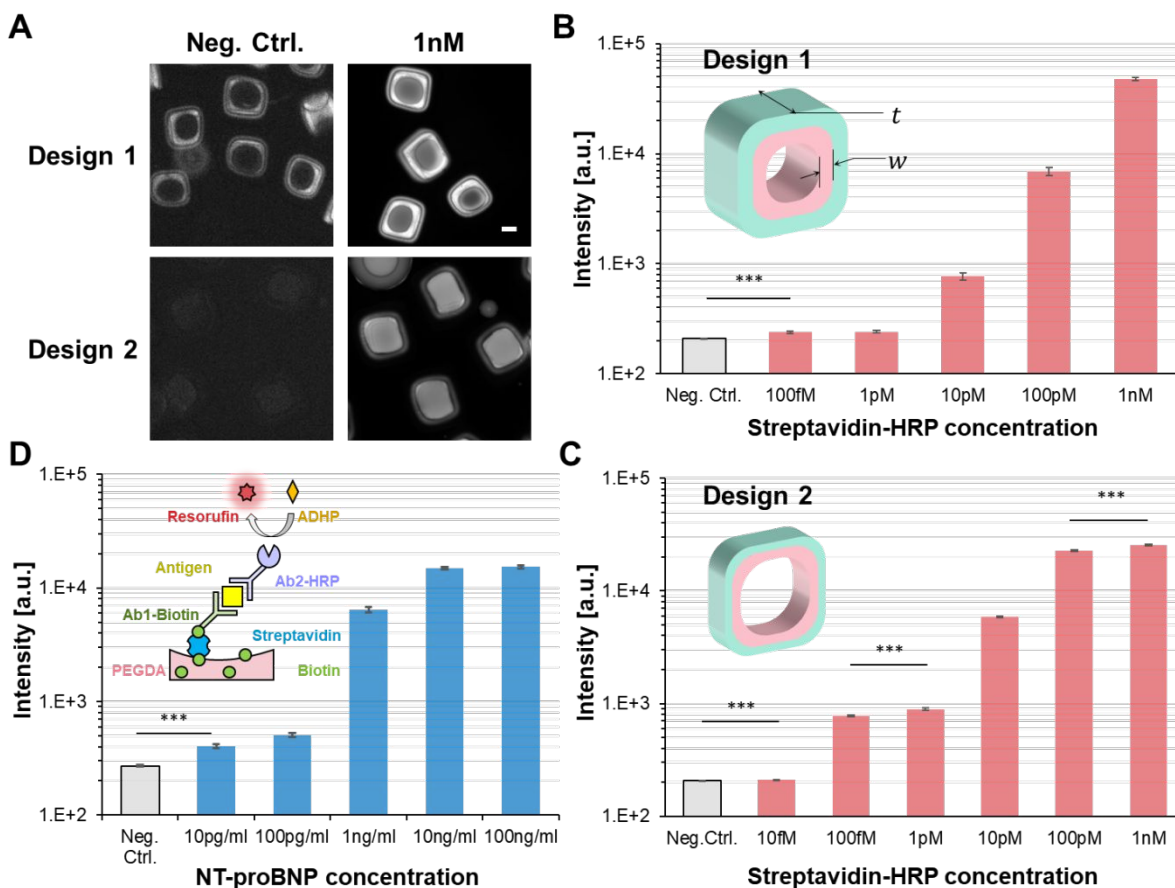


**Figure 5. Amplified assay performance in droplets.** (A) Microscopic images of QuantaRed assay results using two O-shaped particle designs for two concentrations of streptavidin-HRP, i.e., negative control and 1 nM. The look-up table was adjusted to be the same for each condition for visibility. The scale bar represents 100  $\mu\text{m}$ . (B-C) Mean amplified intensity across a population of droplets as a function of concentration of streptavidin-HRP using (B) particle design 1 (N=11-38) and (C) particle design 2 (N=307-382), each tuned by varying the thickness ( $t$ ) and width ( $w$ ) of the internal PEG layer. (D) Mean amplified fluorescent intensity across a population of droplets as a function of concentration of NT-proBNP. Data reported in (A-D) were obtained after 45 min of reaction. Error bars in (B-D) represent standard error. \*\*\* represents  $p < 0.001$ .

### Supporting Information.

The following files are available free of charge.

A PDF file containing additional figures, simulations, discussions and experimental details.

**Corresponding Author**

\* E-mail: dicarlo@ucla.edu

**Author Contributions**

† G.D. and M.O. contributed equally to this work.

G.D., M.O., C.-Y.W, and D.D. curated data. G.D., M.O., and C.-Y.W, performed the investigation. G.D., and M.O. conducted formal analysis. G.D., M.O., and D.D. wrote the original draft. D.D. acquired the funding. The manuscript was written through contributions of all authors. All authors have given approval to the final version of the manuscript.

**ACKNOWLEDGMENT**

This project is supported by the NSF-Engineering Research Center for Precise Advanced Technologies and Health Systems for Underserved Populations (PATHS-UP) - Award Number 1648451. We also acknowledge the Simons Foundation Math+X Investigator Award #510776.

## REFERENCES

- [1] Y. Minagawa, H. Ueno, K. V. Tabata, H. Noji, *Lab Chip* **2019**, *19*, 2678.
- [2] Q. Zhu, L. Qiu, B. Yu, Y. Xu, Y. Gao, T. Pan, Q. Tian, Q. Song, W. Jin, Q. Jin, Y. Mu, *Lab Chip* **2014**, *14*, 1176.
- [3] D. Witters, B. Sun, S. Begolo, J. Rodriguez-Manzano, W. Robles, R. F. Ismagilov, *Lab Chip* **2014**, *14*, 3225.
- [4] V. Yelleswarapu, J. R. Buser, M. Haber, J. Baron, E. Inapuri, D. Issadore, *Proc. Natl. Acad. Sci. U. S. A.* **2019**, *116*, 4489.
- [5] M. T. Guo, A. Rotem, J. A. Heyman, D. A. Weitz, *Lab Chip* **2012**, *12*, 2146.
- [6] S.-Y. Teh, R. Lin, L.-H. Hung, A. P. Lee, *Lab Chip* **2008**, *8*, 198.
- [7] K. W. Bong, J. Lee, P. S. Doyle, *Lab Chip* **2014**, *14*, 4680.
- [8] S. W. Song, S. D. Kim, D. Y. Oh, Y. Lee, A. C. Lee, Y. Jeong, H. J. Bae, D. Lee, S. Lee, J. Kim, S. Kwon, *Adv. Sci.* **2019**, *6*, 1801380.
- [9] S. E. Chung, J. Kim, D. Y. Oh, Y. Song, S. H. Lee, S. Min, S. Kwon, *Nat. Commun.* **2014**, *5*, 1.
- [10] J. Lee, P. W. Bisso, R. L. Srinivas, J. J. Kim, A. J. Swiston, P. S. Doyle, *Nat. Mater.* **2014**, *13*, 524.
- [11] S. A. Dunbar, *Clin. Chim. Acta* **2006**, *363*, 71.
- [12] H. Lee, J. Kim, H. Kim, J. Kim, S. Kwon, *Nat. Mater.* **2010**, *9*, 745.
- [13] Y. Song, Y. Jeong, T. Kwon, D. Lee, D. Y. Oh, T. J. Park, J. Kim, J. Kim, S. Kwon, *Lab Chip* **2017**, *17*, 429.
- [14] D. J. Collins, A. Neild, A. DeMello, A.-Q. Liu, Y. Ai, *Lab Chip* **2015**, *15*, 3439.
- [15] A. S. Basu, *SLAS Technol. Transl. Life Sci. Innov.* **2017**, *22*, 369.

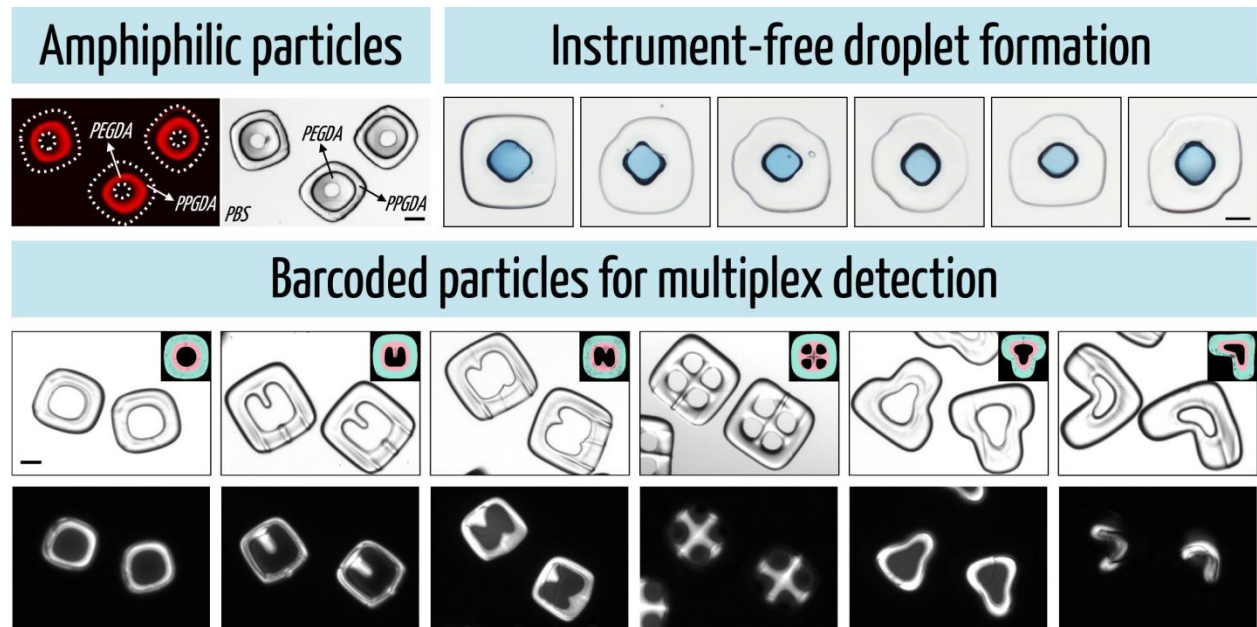
- [16] A. S. Basu, *SLAS Technol. Transl. Life Sci. Innov.* **2017**, *22*, 387.
- [17] R. Novak, Y. Zeng, J. Shuga, G. Venugopalan, D. A. Fletcher, M. T. Smith, R. A. Mathies, *Angew. Chemie Int. Ed.* **2011**, *50*, 390.
- [18] M. N. Hatori, S. C. Kim, A. R. Abate, *Anal. Chem.* **2018**, *90*, 9813.
- [19] P. Gruner, B. Riechers, B. Semin, J. Lim, A. Johnston, K. Short, J.-C. Baret, *Nat. Commun.* **2016**, *7*, 10392.
- [20] Y. Chen, A. Wijaya Gani, S. K. Y. Tang, *Lab Chip* **2012**, *12*, 5093.
- [21] D. Dendukuri, D. C. Pregibon, J. Collins, T. A. Hatton, P. S. Doyle, *Nat. Mater.* **2006**, *5*, 365.
- [22] D. C. Pregibon, M. Toner, P. S. Doyle, *Science* **2007**, *315*, 1393.
- [23] D. Dendukuri, T. A. Hatton, P. S. Doyle, *Langmuir* **2007**, *23*, 4669.
- [24] L. A. Shaw, S. Chizari, M. Shusteff, H. Naghsh-Nilchi, D. Di Carlo, J. B. Hopkins, *Opt. Express* **2018**, *26*, 13543.
- [25] S. E. Chung, W. Park, S. Shin, S. A. Lee, S. Kwon, *Nat. Mater.* **2008**, *7*, 581.
- [26] D. Dendukuri, S. S. Gu, D. C. Pregibon, T. A. Hatton, P. S. Doyle, *Lab Chip* **2007**, *7*, 818.
- [27] R. F. Shepherd, P. Panda, Z. Bao, K. H. Sandhage, T. A. Hatton, J. A. Lewis, P. S. Doyle, *Adv. Mater.* **2008**, *20*, 4734.
- [28] K. W. Bong, D. C. Pregibon, P. S. Doyle, *Lab Chip* **2009**, *9*, 863.
- [29] D. K. Hwang, J. Oakey, M. Toner, J. A. Arthur, K. S. Anseth, S. Lee, A. Zeiger, K. J. Van Vliet, P. S. Doyle, *J. Am. Chem. Soc.* **2009**, *131*, 4499.
- [30] K. W. Bong, K. T. Bong, D. C. Pregibon, P. S. Doyle, *Angew. Chemie* **2010**, *122*, 91.
- [31] A. L. Thangawng, P. B. Howell Jr, J. J. Richards, J. S. Erickson, F. S. Ligler, *Lab Chip* **2009**, *9*, 3126.

- [32] M. Rhee, P. M. Valencia, M. I. Rodriguez, R. Langer, O. C. Farokhzad, R. Karnik, *Adv. Mater.* **2011**, *23*, H79.
- [33] K. W. Bong, J. Xu, J.-H. Kim, S. C. Chapin, M. S. Strano, K. K. Gleason, P. S. Doyle, *Nat. Commun.* **2012**, *3*, 805.
- [34] H. Kim, J. Ge, J. Kim, S. E. Choi, H. Lee, H. Lee, W. Park, Y. Yin, S. Kwon, *Nat. Photonics* **2009**, *3*, 534.
- [35] S. Habasaki, W. C. Lee, S. Yoshida, S. Takeuchi, *Small* **2015**, *11*, 6391.
- [36] Z. Wu, Y. Zheng, L. Lin, S. Mao, Z. Li, J. Lin, *Angew. Chemie* **2020**, *132*, 2245.
- [37] R. Yuan, M. B. Nagarajan, J. Lee, J. Voldman, P. S. Doyle, Y. Fink, *Small* **2018**, *14*, 1803585.
- [38] C.-Y. Wu, K. Owsley, D. Di Carlo, *Adv. Mater.* **2015**, *27*, 7970.
- [39] K. S. Paulsen, D. Di Carlo, A. J. Chung, *Nat. Commun.* **2015**, *6*, 6976.
- [40] C.-Y. Wu, D. Stoecklein, A. Kommajosula, J. Lin, K. Owsley, B. Ganapathysubramanian, D. Di Carlo, *Microsystems Nanoeng.* **2018**, *4*, 21.
- [41] K. S. Paulsen, Y. Deng, A. J. Chung, *Adv. Sci.* **2018**, *5*, 1800252.
- [42] C. H. Chen, R. K. Shah, A. R. Abate, D. A. Weitz, *Langmuir* **2009**, *25*, 4320.
- [43] Y. Zhao, Y. Cheng, L. Shang, J. Wang, Z. Xie, Z. Gu, *Small* **2015**, *11*, 151.
- [44] W. Park, S. Han, H. Lee, S. Kwon, *Microfluid. Nanofluidics* **2012**, *13*, 511.
- [45] S. A. Lee, S. E. Chung, W. Park, S. H. Lee, S. Kwon, *Lab Chip* **2009**, *9*, 1670.
- [46] M. Ouyang, D. Di Carlo, *Biosens. Bioelectron.* **2019**, *132*, 162.
- [47] T. J. Baek, N. H. Kim, J. Choo, E. K. Lee, G. H. Seong, *J. Microbiol. Biotechnol.* **2007**, *17*, 1826.
- [48] W. Lee, D. Choi, J.-H. Kim, W.-G. Koh, *Biomed. Microdevices* **2008**, *10*, 813.

- [49] H. E. Muñoz, C. T. Riche, J. E. Kong, M. van Zee, O. B. Garner, A. Ozcan, D. Di Carlo, *ACS Sensors* **2020**, acssensors.9b01974.
- [50] M. Xiao, K. Zou, L. Li, L. Wang, Y. Tian, C. Fan, H. Pei, *Angew. Chemie* **2019**, ange.201906438.
- [51] S. K. Küster, S. R. Fagerer, P. E. Verboket, K. Eyer, K. Jefimovs, R. Zenobi, P. S. Dittrich, *Anal. Chem.* **2013**, *85*, 1285.
- [52] M. Pabst, S. R. Fagerer, R. Köhling, S. K. Küster, R. Steinhoff, M. Badertscher, F. Wahl, P. S. Dittrich, K. Jefimovs, R. Zenobi, *Anal. Chem.* **2013**, *85*, 9771.
- [53] Q. Wei, H. Qi, W. Luo, D. Tseng, S. J. Ki, Z. Wan, Z. Göröcs, L. A. Bentolila, T.-T. Wu, R. Sun, A. Ozcan, *ACS Nano* **2013**, *7*, 9147.
- [54] H. Zhu, O. Yaglidere, T.-W. Su, D. Tseng, A. Ozcan, *Lab Chip* **2011**, *11*, 315.
- [55] M. Ouyang, D. Tu, L. Tong, M. Sarwar, C. Li, G. L. Coté, D. Di Carlo, **n.d.**
- [56] S. R. Opperwall, A. Divakaran, E. G. Porter, J. A. Christians, A. J. DenHartigh, D. E. Benson, *ACS Nano* **2012**, *6*, 8078.
- [57] Z. Gao, H. Ye, D. Tang, J. Tao, S. Habibi, A. Minerick, D. Tang, X. Xia, *Nano Lett.* **2017**, *17*, 5572.
- [58] W. R. Algar, A. Khachatryan, J. S. Melinger, A. L. Huston, M. H. Stewart, K. Susumu, J. B. Blanco-Canosa, E. Oh, P. E. Dawson, I. L. Medintz, *J. Am. Chem. Soc.* **2017**, *139*, 363.
- [59] D. M. Rissin, C. W. Kan, T. G. Campbell, S. C. Howes, D. R. Fournier, L. Song, T. Piech, P. P. Patel, L. Chang, A. J. Rivnak, E. P. Ferrell, J. D. Randall, G. K. Provuncher, D. R. Walt, D. C. Duffy, *Nat. Biotechnol.* **2010**, *28*, 595.
- [60] J. E. Kong, Q. Wei, D. Tseng, J. Zhang, E. Pan, M. Lewinski, O. B. Garner, A. Ozcan, D. Di Carlo, *ACS Nano* **2017**, *11*, 2934.

- [61] T. Konry, A. Golberg, M. Yarmush, *Sci. Rep.* **2013**, *3*, 3179.
- [62] E. Z. Macosko, A. Basu, R. Satija, J. Nemesh, K. Shekhar, M. Goldman, I. Tirosh, A. R. Bialas, N. Kamitaki, E. M. Martersteck, J. J. Trombetta, D. A. Weitz, J. R. Sanes, A. K. Shalek, A. Regev, S. A. McCarroll, *Cell* **2015**, *161*, 1202.
- [63] N. Nitta, T. Iino, A. Isozaki, M. Yamagishi, Y. Kitahama, S. Sakuma, Y. Suzuki, H. Tezuka, M. Oikawa, F. Arai, T. Asai, D. Deng, H. Fukuzawa, M. Hase, T. Hasunuma, T. Hayakawa, K. Hiraki, K. Hiramatsu, Y. Hoshino, M. Inaba, Y. Inoue, T. Ito, M. Kajikawa, H. Karakawa, Y. Kasai, Y. Kato, H. Kobayashi, C. Lei, S. Matsusaka, H. Mikami, A. Nakagawa, K. Numata, T. Ota, T. Sekiya, K. Shiba, Y. Shirasaki, N. Suzuki, S. Tanaka, S. Ueno, H. Watarai, T. Yamano, M. Yazawa, Y. Yonamine, D. Di Carlo, Y. Hosokawa, S. Uemura, T. Sugimura, Y. Ozeki, K. Goda, *Nat. Commun.* **2020**, *11*, 1.

## Entry for the Table of Contents



Uniform fluid compartments are formed inside particles designed with concentric hydrophilic and hydrophobic polymers following simple fluid exchange steps. Fluid volumes templated by the particles support enzymatic reactions without cross talk. Shape-coded particles that enable multiplexing are manufactured in bulk using 3D printed microfluidic networks and could be easily distributed to help democratize cutting-edge biological assays.